

The Catalytic Oxidation of Propylene

IX. The Kinetics and Mechanism over β -Bi₂Mo₂O₉

JOHN R. MONNIER¹ AND GEORGE W. KEULKS

Department of Chemistry, Laboratory for Surface Studies, University of Wisconsin-Milwaukee, Milwaukee, Wisconsin 53201

Received February 27, 1980; revised September 22, 1980

The kinetics and mechanism of propylene oxidation over β -Bi₂Mo₂O₉ from 300 to 470°C have been investigated. By using oxygen-18 and deuterated propylenes under steady-state reaction conditions and temperatures ranging from 350 to 450°C, it was determined that the selective oxidation of propylene to acrolein over the β -phase occurs via the redox mechanism through the involvement of numerous sublayers of lattice oxygen. From the kinetic and isotopic data it was learned that the kinetics and energetics of propylene oxidation over the β -phase can be completely described in terms of the coupled kinetics of catalyst reduction and reoxidation. At the higher temperatures in which the rate of acrolein formation is limited by catalyst reduction, the apparent activation energy is approximately 20 kcal/mole and is indicative of allyl formation from adsorbed propylene. At lower temperatures the rate of acrolein formation is limited by catalyst reoxidation and the apparent activation energy is approximately 43 kcal/mole. The kinetic dependencies of oxygen and propylene also reflect the changes in the rate-determining step of the reaction. Carbon dioxide is produced from both the consecutive oxidation of acrolein and the oxidation of a hydrocarbon residue which is present on the surface of the catalyst at steady-state conditions; the former pathway predominates at low temperatures (below 400°C), while the latter pathway contributes significantly at high temperatures to carbon dioxide formation. Both pathways utilize only lattice oxygen; the extent of lattice oxygen participation is approximately the same as acrolein formation.

INTRODUCTION

The kinetics and mechanism of propylene oxidation over bismuth molybdate catalysts have been studied in considerable detail and are the subject of several extensive reviews (1-4). A number of phases have been detected in the bismuth molybdate system, but only three phases are generally accepted as exhibiting superior catalytic activity and selectivity. These phases are the α -phase, Bi₂Mo₃O₁₂; the β -phase, Bi₂Mo₂O₉; and the γ -phase, Bi₂MoO₆. While the α - and γ -phases of bismuth molybdate have been thoroughly investigated (5, 6), the β -phase modification, β -Bi₂Mo₂O₉, has received much less attention. This is in part due to

the assumption by some researchers (7-9) that the β -phase is only a mixture of the α - and γ -phases and not a distinct phase, while other investigators (10-12) believe the β -phase is unstable at the elevated temperatures required for propylene oxidation. However, recent work by Monnier (13) has verified that the β -phase is a pure phase of the bismuth molybdate system and is stable at the temperatures required for an in-depth study of the kinetics and mechanism of propylene oxidation.

Therefore, we have investigated the kinetics and mechanism of propylene oxidation over the β -phase to determine whether the kinetics and mechanistic parameters are similar to those for the α - and γ -phases, discussed by Krenzke and Keulks (5, 6).

It has been generally concluded that the first and usually rate-determining step for the selective oxidation of propylene over

¹ Present address: Kodak Research Laboratory, Eastman Kodak Company, 1669 Lake Avenue, Rochester, New York 14651.

bismuth molybdate catalysts is the abstraction of a hydrogen from the allylic methyl group of propylene (1, 2). A second hydrogen is abstracted from either equivalent end of the adsorbed allylic species before the incorporation of a lattice oxide ion to form acrolein. This is called the redox mechanism since the catalyst itself serves as the oxidizing agent, while the gas phase oxygen reoxidizes the reduced catalyst.

Another possible mechanism for the selective oxidation of propylene is the hydroperoxide pathway, in which adsorbed molecular oxygen interacts with the adsorbed allylic species to form a surface peroxide or hydroperoxide that decomposes to form acrolein. Although this mechanistic pathway has been observed for propylene oxidation over nonreducible metal oxides (14, 15) and noble metals (16, 17), Daniel *et al.* (18) observed that allyl hydroperoxide was formed at temperatures up to 450°C on an unspecified phase of bismuth molybdate. This intermediate could either dissociate on the surface to form acrolein or desorb into the gas phase and initiate homogeneous gas phase oxidation reactions. Only small amounts of acrolein were formed from this pathway; the great majority was formed from lattice oxygen via the redox pathway.

The first order dependency on propylene pressure for acrolein formation (at $T > 400^\circ\text{C}$) has been generally viewed as a consequence of the dissociative adsorption of propylene to form the π -allylic species as the rate-determining step (6, 19). The zero-order kinetics for oxygen dependency over the same temperature range has been attributed to direct participation of lattice oxygen in acrolein formation and the subsequent rapid reoxidation of the catalyst by gas phase oxygen (6, 19). The similar kinetic dependencies for CO_2 formation have been reasoned to be the result of the consecutive pathway of CO_2 formation from adsorbed acrolein (6, 19-22).

Variation of the observed kinetic dependencies for product formation at lower tem-

peratures (partial order for O_2 dependency and zero or partial order for propylene dependency) has been reasoned to be the result of either a change in the rate-determining step of the reaction to the desorption of acrolein (23, 24) or a change in the mechanism of the reaction (25). The same arguments have been used to describe the changes of activation energies for acrolein and carbon dioxide formation at lower temperatures.

Krenzke and Keulks (6) recently studied the kinetics of propylene oxidation over $\alpha\text{-Bi}_2\text{Mo}_3\text{O}_{12}$ and $\gamma\text{-Bi}_2\text{MoO}_6$ from 325 to 475°C. The apparent activation energies for acrolein formation varied from 15 to 18 kcal/mole at temperatures greater than 400°C to 43 to 53 kcal/mole at lower temperatures. The reaction orders for propylene and oxygen changed from first order in propylene and zero in oxygen in the high-temperature region to zero or partial orders in propylene and partial order in oxygen pressure in the low-temperature region. They explained these changes in the kinetic parameters in terms of the coupled kinetics of catalyst reduction and reoxidation.

EXPERIMENTAL

A. Catalyst Preparation

The β -phase catalyst used in this study was prepared according to the method of Grzybowska *et al.* (26). Details regarding the purity and stability of this particular preparation have been discussed in detail by Monnier (13).

B. Apparatus

The reactor system used for all experiments has been discussed earlier by Krenzke and Keulks (5).

The feed gases, oxygen (Airco, 99.6%), propylene (Linde, C. P. grade), and helium (Airco, 99.99%) were used with no further purification. The individual gas flows were controlled by Tylan FC-260 mass flow controllers.

The isotopically labeled gases used in this study were oxygen-18 (99 at% ^{18}O) from BOC Ltd. Prochem., London, England, 2,3,3,3- $\text{d}_4\text{-C}_3\text{D}_4\text{H}_2$ (98.1 at% labeled), and 1,1,2- $\text{d}_3\text{-C}_3\text{D}_3\text{H}_3$ (98.0 at% labeled), the latter two gases being purchased from Merck, Sharp, and Dohme, Canada Ltd., Montreal, Canada. These labeled compounds were introduced to the feed stream by a variable speed syringe pump (Sage Instruments, model 341) equipped with a 10 cm^3 Hamilton gas-tight syringe.

The feed gas composition and product distribution were analyzed by a dual-column Packard 417 Becker gas chromatograph using two $1/4'' \times 6'$ columns packed with 80–100 mesh Porapak R. Peak areas were converted to micromoles using a Spectra-Physics Autolab System I computing integrator.

A Bendix MA-1 time of flight mass spectrometer was used to analyze the isotopic distribution of reaction products during the tracer experiments. The mass spectrometer was directly coupled to the reactor exit by a Granville-Phillips Series 203 variable leak valve.

The output of the mass spectrometer was recorded using a Columbia Scientific Industries CSI-260 digital readout system which digitally recorded the maximum peak heights for all m/e values over the desired scan range.

C. Experimental Technique

1. *Kinetic data.* Before any kinetic data were obtained, all catalysts were allowed to reach steady-state activity at 425°C in an oxidizing atmosphere. In order to ensure differential flow conditions, conversion was kept at less than 7% and small catalyst charges were used in the micro-reactor. A 0.250 g charge was commonly used at 325°C with total flow of 20 SCCM. (SCCM will be used throughout to denote flow rates in cm^3/min at standard temperature and pressure.) At higher temperatures a smaller portion of the original catalyst charge

and/or higher flow rates were used to maintain conversion below 7%.

The reaction orders for C_3H_6 and O_2 were calculated over the approximate temperature range 300–475°C at 25°C intervals. When calculating the pressure dependencies of C_3H_6 at the various temperatures, the O_2 partial pressure was held constant at 0.3 atm (unless otherwise stated) while decreasing the C_3H_6 partial pressure from 0.3 atm; at most temperatures a minimum of four different C_3H_6 pressures were used. For calculation of the oxygen pressure dependencies, the C_3H_6 pressure was held constant at approximately 0.1 atm (unless otherwise stated) while decreasing the O_2 partial pressure from 0.3 atm to 0.1 atm. Thus in all cases, the reaction was carried out in an oxidizing atmosphere.

2. *Oxygen-18 data.* The feed gas composition was 0.1 atm O_2 , 0.1 atm C_3H_6 , and 0.8 atm He at a total flow of 20 SCCM. The size of the catalyst charge was varied to obtain a conversion of 10–20%. This extent of reaction was necessary for an accurate mass spectrometric analysis.

Before an oxygen-18 experiment was performed, the reaction was allowed to reach steady-state conditions. To start the addition of $^{18}\text{O}_2$ to the feed stream, the syringe pump was activated while simultaneously diverting the $^{16}\text{O}_2$ from the feed stream to vent by means of a three-way valve. The flow rates of $^{16}\text{O}_2$ and $^{18}\text{O}_2$ were matched so that oxygen flow remained constant throughout the entire experiment. The matched flow rates and rapid changeover of feed oxygen maintained the previously established steady-state conditions.

During the mass spectrometric analysis, the oxygen-18 concentrations in the gas phase O_2 , CO_2 , and $\text{C}_3\text{H}_4\text{O}$ were determined by repetitively scanning the m/e range 20–65 every 15 sec at 3.5×10^{-6} Torr pressure. A minimum of 15 scans were made during each tracer experiment.

Near the end of the tracer experiment, the product stream was diverted through the Carle switching valves and a gc

analysis was made of the reaction products.

3. *Deuterated propylene data.* The experimental technique was the same as for the oxygen-18 experiments, except the C_3H_6 flow controller was externally connected to the syringe pump assembly.

The rate constants and subsequent primary isotope effects for acrolein and carbon dioxide formation from the deuterated propylene oxidation reactions were calculated from gas chromatographic data.

The deuterium content of acrolein was used to calculate the secondary discrimination effect for acrolein formation. In the case of both $CD_2=CD-CH_3$ and $CD_3-CD=CH_2$, the mass numbers of interest were 59 ($CD_2=CD-CHO$) and 58 ($CH_2=CD-CDO$).

4. *Oxidation of the steady-state catalyst surface.* To prepare the steady-state catalyst surface for oxidation by O_2 , a stream of 0.1 atm O_2 , 0.1 atm C_3H_6 , and 0.8 atm He with a total flow of 20 SCCM was passed over the catalyst at the desired temperature. When mass spectrometric analysis showed a constant conversion and selectivity, the O_2 and C_3H_6 gas flows were diverted to vent, leaving only He flowing over the catalyst. After residual reactants and products were swept from the product flow stream, O_2 was introduced into the He feed by means of the syringe pump. By varying the pumping speed of the syringe pump, the kinetic dependency of O_2 for product formation was calculated. To observe the isotopic distribution of oxygen-18 in the reaction products, $^{18}O_2$ was substituted for $^{16}O_2$ in the feed stream.

5. *Reduction of the steady-state catalyst surface with propylene.* The steady-state surface preparation and apparatus were the same as described for the oxidation experiments. Propylene was introduced into the He feed stream at 2.4 SCCM by means of the syringe pump. The gas chromatograph, rather than the mass spectrometer, was used to analyze the reaction products.

A comparison of steady-state catalytic

activity before and after the C_3H_6 reduction of $\beta-Bi_2Mo_2O_9$ was made to determine whether the catalyst was irreversibly deactivated by C_3H_6 reduction.

Reduction of the catalyst surface by $CD_3-CH=CH_2$ permitted the calculation of the primary isotope effects for CO_2 and acrolein formation.

RESULTS

A. Kinetic Data

The kinetic dependencies of propylene and oxygen for acrolein and carbon dioxide formation were calculated from the following empirical rate equation,

$$\text{rate} = k[C_3H_6]^x[O_2]^y, \quad (1)$$

where k is the rate constant and x and y are the reaction orders for C_3H_6 and O_2 , respectively. A plot of $\ln(\text{rate})$ versus $\ln(\text{concentration of the reaction being varied})$ will give a straight line with a slope equal to the reaction order of that reactant and a y -intercept equal to $\ln k'$, where k' is the product of k and the concentration term for the reactant at constant concentration. The propylene and oxygen dependencies for acrolein formation are presented in Figs. 1 and 2, respectively; the analogous plots for CO_2 formation are not shown but are somewhat similar to Figs. 1 and 2. The reaction orders calculated from the above data are summarized in Table 1. At 350, 375, and 400°C, it is necessary to subdivide the propylene dependencies for CO_2 and C_3H_4O formation into two different propylene partial pressure ranges.

The specific rate constants for C_3H_4O and CO_2 formation were calculated from the empirical rate equation after the reaction orders had been evaluated.

The apparent energies of activation for C_3H_4O and CO_2 formation were determined from Arrhenius plots of the appropriate rate constants. The Arrhenius plots for C_3H_4O and CO_2 formation are presented in Figs. 3 and 4. For the data at 350, 375, 400, and 425°C, the closed circles represent the

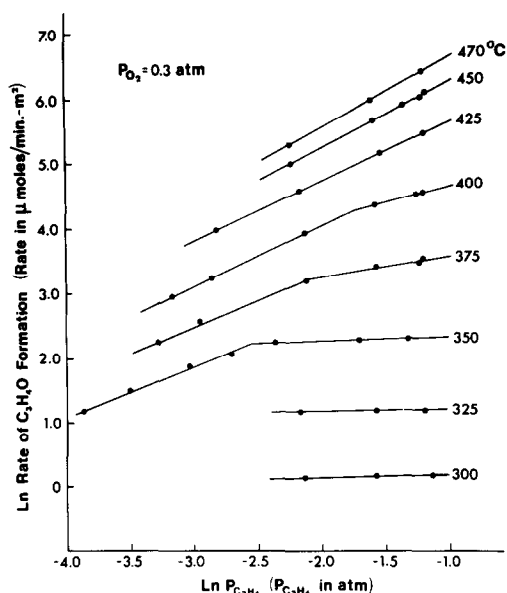


FIG. 1. C_3H_6 dependency for acrolein formation as a function of temperature.

rate constants calculated from the C_3H_6 and O_2 reaction orders at higher C_3H_6 partial pressures while the open circles are for the rate constants calculated at lower C_3H_6

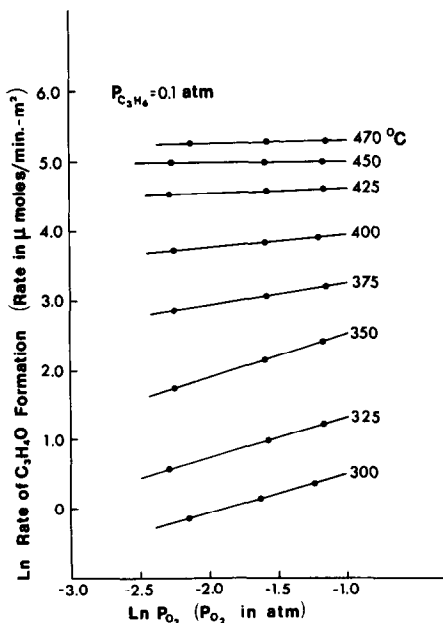


FIG. 2. O_2 dependency for acrolein formation as a function of temperature.

TABLE 1
Reaction Orders for C_3H_6 Oxidation

Temperature ($^{\circ}C$)	C_3H_4O Formation		CO_2 Formation	
	C_3H_6	O_2	C_3H_6	O_2
300	0	0.50	Not enough product	
325	0	0.55	Not enough product	
350	(0.1–0.3 atm C_3H_6)		0.40	0.45
	(0.06–0.1 atm C_3H_6)		0.85	0
			0.40	0.50
375	(0.1–0.3 atm C_3H_6)		0.35	0.30
	(0.04–0.1 atm C_3H_6)		0.90	0.30
400	(0.2–0.3 atm C_3H_6)		0.60	0.20
	(0.04–0.2 atm C_3H_6)		1.0	0.20
425	1.0	0	1.40	0.30
450	1.0	0	1.50	0.30
470	1.0	0	1.50	0.30

partial pressures. The dashed lines are used to connect the open circles.

Each Arrhenius plot is composed of two intersecting lines. For C_3H_4O formation,

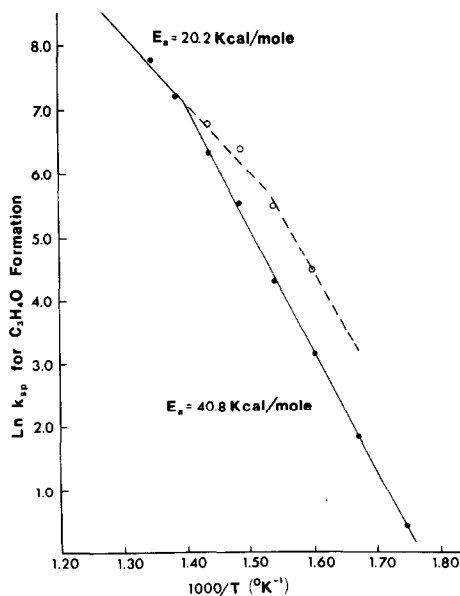


FIG. 3. Arrhenius plot for C_3H_4O formation over $\beta-Bi_2Mo_2O_9$.

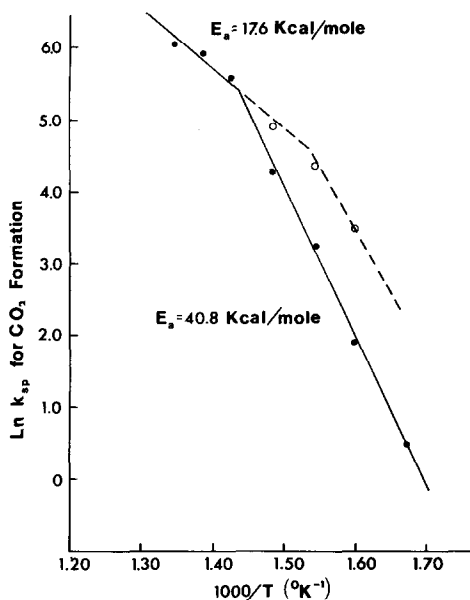


FIG. 4. Arrhenius plot for CO_2 formation over $\beta\text{-Bi}_2\text{Mo}_2\text{O}_9$.

the transition temperature is approximately 435°C and for CO_2 formation, approximately 425°C . For both Figs. 3 and 4, the apparent energies of activation are listed adjacent to their corresponding portions of the Arrhenius plots. In each figure it can be seen that the extension of the Arrhenius plot from higher temperatures to lower temperatures coincides with the dashed line. Thus, by extending the kinetic analysis to lower C_3H_6 partial pressures, it is possible to shift the transition temperature to lower temperatures.

A closer examination of the kinetics for CO_2 and $\text{C}_3\text{H}_4\text{O}$ formation at 350°C is shown in Fig. 5. The C_3H_6 dependencies for $\text{C}_3\text{H}_4\text{O}$ and CO_2 formation were calculated by varying the C_3H_6 partial pressures from 0.02 to 0.3 atm while maintaining the O_2 concentration at 0.3 atm. Likewise, the O_2 dependencies were determined by varying the O_2 pressure from 0.03 to 0.3 atm while holding the C_3H_6 pressure at 0.05 atm. The C_3H_6 and O_2 dependencies are listed adjacent to their respective portions of the curves.

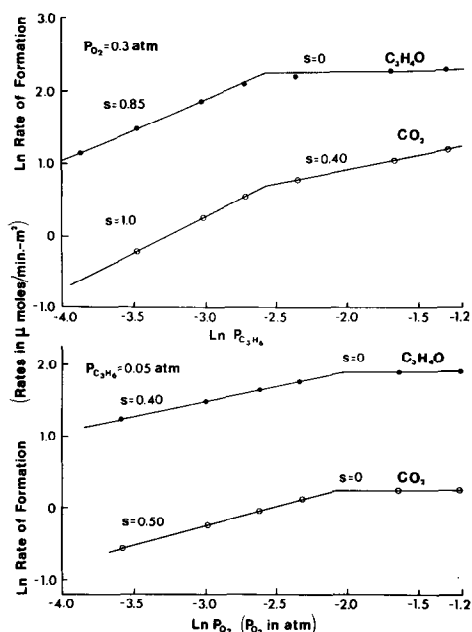


FIG. 5. Extended kinetic analysis of $\text{C}_3\text{H}_4\text{O}$ and CO_2 formation at 350°C .

B. Oxygen-18 Studies

The purpose of using $^{18}\text{O}_2$ as a tracer in the feed stream was to establish in a quantitative manner the source and quantity of oxygen during CO_2 and $\text{C}_3\text{H}_4\text{O}$ formation. This quantity or dilution volume of oxygen adsorbed on the surface or in the bulk of the catalyst that equilibrates with the gas phase $^{18}\text{O}_2$ can be related to the oxygen-18 content of the products and the oxygen flux through the catalyst by assuming the reactive oxygen reservoir is equivalent to an exponential dilution volume (5).

Table 2 summarizes the oxygen-18 incorporation data for $\text{C}_3\text{H}_4\text{O}$ and CO_2 formation at 450, 400, and 350°C from the oxidation of propylene. Oxidation of propylene at 350 and 450°C using equal amounts of $^{18}\text{O}_2$ and $^{16}\text{O}_2$ in the feed stream did not produce any detectable $^{18}\text{O}^{16}\text{O}$ in the reaction effluent, indicating the isotopic exchange reaction $^{16}\text{O}_2 + ^{18}\text{O}_2 \rightleftharpoons 2 ^{18}\text{O}^{16}\text{O}$ did not occur at the reaction conditions used in this study.

To obtain more information about the

TABLE 2

Summary of Oxygen-18 Incorporation Data

Temperature (°C)	Percentage of catalyst oxygen involved in formation of		Number of layers ^a of oxygen involved in formation of	
	C ₃ H ₄ O	CO ₂	C ₃ H ₄ O	CO ₂
450	98	98	312	312
400	56	60	176	190
350	29	32	90	101

^a Calculated from S.A. = 2.3 m²/g and assumption of 1×10^{15} atoms/cm².

low-temperature regions of the Arrhenius plots in Figs. 3 and 4, the oxidation of C₃H₆ was carried out using ¹⁸O₂ at 350°C. The rate constants for C₃H₄O and CO₂ formation using ¹⁸O₂ were calculated from gc analyses (and the previously calculated reaction orders from Table 1) and compared to the analogous rate constants using ¹⁶O₂. If the rate-determining step at low temperatures involves the breaking of the O–O bond, one should expect a kinetic isotope effect since the ¹⁸O–¹⁸O bond is of lower energy than the ¹⁶O–¹⁶O bond. The maximum observable isotope effect is, of course, strongly dependent on the nature of the O₂ species at the transition state. The theoretical kinetic isotope effects were calculated from Raman stretching data for ¹⁶O₂ using the method outlined by Melander (27).

The results in Table 3 summarize the experimental results. Also included are theoretical isotope effects for several different O₂ species from the literature.

A small isotope effect was observed as expected if the rate-determining step involves breaking an O–O bond. It should be noted, however, that the observed isotope effects are the results of five ¹⁸O₂ analyses and five ¹⁶O₂ analyses. Therefore, the results in Table 3 are the averaged isotope effects; however, for each ¹⁸O₂/¹⁶O₂ pair,

TABLE 3

Oxygen Isotope Effects for C₃H₄O and CO₂ Formation at 350°C

Product	Observed isotope effects ^a		
	<i>k</i> ₁ / <i>k</i> ₂		
C ₃ H ₄ O	1.03 to 1.04		
CO ₂	1.02 to 1.03		
Theoretical isotope effects			
Reference	Oxygen species	$\bar{\nu}_1$ (cm ⁻¹)	<i>k</i> ₁ / <i>k</i> ₂
28	Gas phase O ₂	1580	1.11
29	O ₂ ⁻ (in alkali halides)	1140	1.09
30	O ₂ ⁻ (from KO ₂)	1145	1.09
31	O ₂ ²⁻ (from Na ₂ O ₂)	766	1.07
32	Coordinated molecular		
	O ₂ in K ₂ Mo(O ₂) ₂ OF ₂	62	1.07

^a *k*₁ is for ¹⁶O₂ and *k*₂ is for ¹⁸O₂.

there was an observable isotope effect and this value was essentially the same for the five pairs of analyses. Therefore, even though the observed oxygen isotope effects were small, they were reproducible.

C. Oxidation of 2,3,3,3,-d₄ and 1,1,2-d₃ Propylenes

If the rate-determining step of propylene oxidation is abstraction of an allylic hydrogen, then one should expect a full primary kinetic isotope effect for C₃H₄O and CO₂ formation when the allylic position of propylene is completely deuterated. Further, if the rate-determining step remains the same for the entire temperature range investigated, then the full kinetic isotope effect should be observed throughout. The results in Table 4 summarize the observed primary kinetic isotope effects for both 2,3,3,3,-d₄ and 1,1,2-d₃ propylene oxidations at 350, 400, and 450°C. These results are compared to the theoretical primary isotope effects for C–D versus C–H bond breaking in the allylic position. The theoretical values were calculated from Melander's (27) heavy atom residue approximation.

The isotopic distribution of deuterium in acrolein can be used to predict the se-

TABLE 4
Primary Kinetic Isotope Effects^a for 2,3,3,3-d₄ and 1,1,2-d₃ Propylene Oxidation over β -Bi₂Mo₂O₉

	450°C		400°C		350°C	
	Acrolein	CO ₂	Acrolein	CO ₂	Acrolein	CO ₂
	2,3,3,3-d ₄ Propylene					
Theoretical	1.75	1.75	1.92	1.92	2.14	2.14
Observed	1.65	1.65	1.5	1.5	1.4	1.4
Observed/ theoretical × 100	85%	85%	54%	54%	35%	35%
	1,1,2-d ₃ Propylene					
Theoretical	1.00	1.00	1.00	1.00	1.00	1.00
Observed	1.0	1.0	1.0	1.0	1.0	1.0

^a The data are presented as k_H/k_D .

quence of the second hydrogen abstraction and oxygen addition to form acrolein. The results in Table 5 give the theoretical and experimental deuterium distributions of acrolein produced from oxidation of 2,3,3,3-d₄ propylene and 1,1,2-d₃ propylene. The theoretical distribution is calculated from the equation used for the calculation of the primary kinetic isotope effect and is based on the assumption that the second hydrogen atom is abstracted from the symmetrical allylic species before the addition of an oxygen atom. The theoretical deuterium distributions are the same for both deuterated propylene tracers, since the allylic intermediate common to both is CD₂=CD=CH₂.

It should be noted that the only deuterated acroleins formed were CD₂=CDCHO and CH₂=CDCDO, indicating that no intermolecular deuterium exchange had occurred.

D. Reduction of β -Bi₂Mo₂O₉ by Propylene

The oxidation of propylene at 350°C was more closely examined by comparing the initial rates of C₃H₄O and CO₂ formation over a steady-state catalyst surface in a C₃H₆, He-feed stream with the corresponding rates in an O₂, C₃H₆, He-feed stream. Steady-state product analyses were made before and after the reaction of propylene

with β -Bi₂Mo₂O₉ in the absence of O₂. The latter steady-state analysis indicated the catalyst was not irreversibly reduced (and subsequently deactivated) during the reduction of the catalyst by C₃H₆. The results are shown in the upper portion of Table 6 and reveal comparable rates of formation of C₃H₄O in both the presence and absence of gas phase O₂. The data for CO₂ formation do not give such good agreement and are a result of the very small amounts of CO₂ formed under these reaction conditions. The selectivity to acrolein formation insured adequate amounts of acrolein for gc analyses. Three C₃H₆, He flow analyses were made (catalyst was reoxidized in the O₂, C₃H₆, He-feed stream to steady-state conditions between C₃H₆, He flow analyses), and the rates of acrolein formation were very reproducible.

The primary kinetic isotope effects for acrolein and CO₂ formation during catalyst reduction by propylene were calculated by substituting 2,3,3,3-d₄ propylene for C₃H₆ in the C₃H₆, He-feed stream. These results are presented in the lower portion in Table 6.

E. Oxidation of the Steady-State β -Bi₂Mo₂O₉ Surface

The reaction orders of C₃H₆ and O₂ for CO₂ formation in Table 1 are different from

the analogous reaction orders for C_3H_4O formation. Therefore, the oxidation by gas phase O_2 of a previously established steady-state surface was performed at 350 and 425°C to examine the source of the CO_2 produced during the steady-state oxidation of C_3H_6 and to explain the unusual O_2 and C_3H_6 reaction orders. The reaction products were limited to CO_2 and H_2O with no detectable amounts of acrolein. Significant amounts of CO_2 were produced during oxidation of the catalyst surface, indicating a considerable hydrocarbon build-up on the surface. The fractions of CO_2 produced by oxidation of the steady-state surface at 350 and 425°C were approximately 15 and 30%, respectively, of the amounts of CO_2 produced during the steady-state oxidation of C_3H_6 . Space-velocity measurements of the rates of formation of acrolein and CO_2 and the conversion of propylene at 425°C indicated that the hydrocarbon deposit on the surface of the catalyst was not due to diffusion limitations of oxidation products

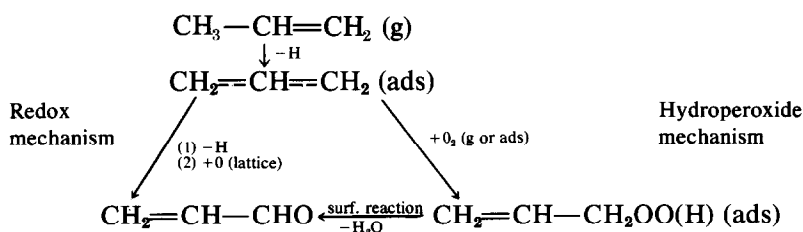
from the catalyst. This is the expected result for a catalyst such as $\beta-Bi_2Mo_2O_9$ with negligible pore volume and low surface area.

The O_2 dependencies for CO_2 formation during the oxidation of the steady-state surface at 350 and 425°C are presented in Table 7. The C_3H_6 dependencies were not determined since there was no direct way to determine the rate of surface build-up. The source of the oxygen in the CO_2 was determined by replacing the $^{16}O_2$ in the feed stream with $^{18}O_2$. The isotopic distribution of CO_2 is also listed in Table 7.

DISCUSSION

A. The Mechanistic Model

The relationship of acrolein and CO_2 formation as they are related to the kinetic and tracer results will be discussed within the framework of the mechanistic model which has been proposed earlier (33).



The expected kinetic and isotopic results that one should expect for the above scheme can be stated in the following manner:

(1) The initial and rate-determining step is the abstraction of an allylic hydrogen to form a symmetrical allylic species on the surface. Thus, one should expect a first-order kinetic dependency on propylene partial pressure and a full kinetic isotope effect if $CH_2=CD_2$ is substituted for non-deuterated propylene.

(2) After formation of the allylic species, the reaction may proceed via the redox mechanism or hydroperoxide mechanism to produce acrolein. If oxygen incorporation occurs immediately after the formation of the allylic species (hydroperoxide pathway) each end of the allylic intermediate will react with equal probability, yielding equal amounts of $CD_2=CDCHO$ and $CH_2=CDCDO$. If, however, abstraction of a second hydrogen (or deuterium) occurs before oxygen incorporation, the amounts of acrolein formed by the loss of hydro-

TABLE 5
Deuterium Distribution^a in Acrolein from Oxidation of 2,3,3,3-d₄ Propylene and 1,1,2-d₃ Propylene

	450°C		400°C		350°C	
	CD ₂ =CDCHO	CH ₂ =CDCDO	CD ₂ =CDCHO	CH ₂ =CDCDO	CD ₂ =CDCHO	CH ₂ =CDCDO
Theoretical	64	36	66	34	68	32
Observed from CH ₂ =CDD ₃ oxidation	65	35	66	34	68	32
Observed from CD ₂ =CDCH ₃ oxidation	66	34	65	35	68	32

^a Data are expressed as percentage of deuterated species.

TABLE 6

Summary of β -Bi₂Mo₂O₉ Reduction by Propylene at 350°C

Reaction condition (in order of experiments)	Rates of formation (μ mole/min-m ²)	
	Acrolein	CO ₂
Steady-state oxidation of C ₃ H ₆	6.16	2.55
Reduction of catalyst by C ₃ H ₆	6.18	3.7
Steady-state oxidation of C ₃ H ₆	6.46	2.52

	k_H/k_D ratios	
	Acrolein	CO ₂
Theoretical	2.14	2.14
Observed ^a	2.30	3.0

^a Based on four experiments.

gen (CD₂=CDCHO) and deuterium (CH₂=CDCDO) will be governed by the secondary discrimination effect.

(3) A more definitive means of distinguishing between the redox mechanism and hydroperoxide mechanism is to determine the source of oxygen in the products. The redox pathway incorporates lattice O²⁻ into acrolein while an adsorbed oxygen species is involved in the hydroperoxide route. Thus, if propylene is oxidized in the pres-

TABLE 7

Summary of Results from the Oxidation of the Steady-State Surface of β -Bi₂Mo₂O₉

Temperature (°C)	O ₂ order for CO ₂	Isotopic distribution (mole%)		
		CO ₂ (44)	CO ₂ (46)	CO ₂ (48)
350	0.30	75	13	12
425	0.25	>90	<5	<5

ence of $^{18}\text{O}_2$, the rate of oxygen-18 incorporation into acrolein (as well as CO_2) can be used to determine the quantity of catalyst oxygen involved in product formation. A quantity of oxygen equivalent to a monolayer or less illustrates that adsorbed oxygen (hydroperoxide pathway) is the active species, while quantities equivalent to several sublayers of oxygen are indicative of the participation of lattice oxygen (redox pathway).

(4) The participation of lattice oxygen for product formation via the redox pathway implies a zero-order oxygen dependency for propylene oxidation, assuming that catalyst reoxidation occurs at a rate greater than the formation of the allylic species. Further, one should not expect a kinetic isotope effect for O-O bond breaking if $^{16}\text{O}_2$ is replaced by $^{18}\text{O}_2$ in the gas phase.

B. Kinetics and Mechanism of Acrolein Formation

The results in Figs. 1 and 2 and Table 1 reveal that the reaction kinetics are not first order in propylene and zero order in oxygen partial pressures throughout the complete temperature range, indicating an apparent deviation from the redox pathway. However, at temperatures of approximately 425°C or greater, the β -phase exhibits the kinetics expected of the redox pathway. Batist *et al.* (23, 24) have reported first-order and zero-order kinetics for 1-butene and oxygen pressures, respectively, during the oxidation of 1-butene from 308 to 425°C over the β -phase. In addition, Haber (34) found that the reduction of the β -phase, presumably at 440°C , exhibited first-order propylene kinetics, although the reduction kinetics may not be equivalent to those for the steady-state oxidation of propylene. The observed kinetics most closely resemble those reported by Krenzke and Keulks (6) for the oxidation of propylene over the α - and γ -phases. For these catalysts, they found the reaction orders changed from first order in propylene and zero order in oxy-

gen above 400°C to zero or partial order in propylene and partial order in oxygen pressures below 400°C .

In addition to the temperature dependency of the kinetics, Figs. 1 and 5 illustrate the kinetics are dependent upon the partial pressure range of the reactant being investigated. At 350°C , it is possible to change the propylene dependency from zero to approximately first order (0.85) by decreasing the pressure of propylene from 0.3 to 0.02 atm while maintaining a constant oxygen pressure of 0.3 atm. A comparable effect is observed for the oxygen dependency by varying the oxygen pressure from 0.3 to 0.03 atm while holding the propylene at 0.05 atm. Therefore, by proper selection of the propylene and oxygen partial pressures at 350°C , it is possible to obtain the kinetics normally observed above 425°C and usually linked with the redox mechanism.

This complex isothermal kinetic dependency most likely explains the discrepancy between the lower temperature kinetics found in this study and those reported by Batist (23, 24) for the β -phase at lower temperatures. Likewise, because both the propylene and oxygen pressures were varied only between 0.1 and 0.3 atm, Krenzke and Keulks (6) observed no isothermal breaks in the reaction orders during the investigation of the α - and γ -phases.

The Arrhenius curve for acrolein formation in Fig. 3 reflects the observed propylene dependencies of Table 1. Recalculation of k_{sp} values using the reaction orders obtained at lower propylene partial pressures gives the data points connected by the dashed line. The transition temperature has been shifted to 350°C from the previous values of approximately 435°C . The apparent activation energy of 20.2 kcal/mole at temperatures above 435°C (or 350°C , using lower propylene pressures) is indicative of the redox mechanism and is in general agreement with the value of 15 kcal/mole reported by Haber (34) during β -phase reduction by propylene. For temperatures

greater than 400°C, Krenzke and Keulks (6) obtained values of 15 and 18 kcal/mole for the γ - and α -phases, respectively.

The unusual propylene and oxygen dependencies and the break in the Arrhenius plot indicate an apparent change in the rate-determining step and/or a change in the mechanism of propylene oxidation. The use of oxygen-18 and deuterated propylene isotope tracers can be used to resolve the observed kinetic parameters.

The oxygen-18 data which are summarized in Table 2 show that there is extensive lattice O^{2-} participation for acrolein formation at all temperatures. However, only at 450°C with 98% lattice O^{2-} participation can it be conclusively stated that only lattice O^{2-} is involved in acrolein formation. At 400 and 350°C, acrolein formation from both the redox and hydroperoxide pathways cannot be excluded, since less than 100% of the lattice O^{2-} participates in acrolein formation. However, because of the thermally activated nature of O^{2-} or V_o (oxide vacancy) mobility, one would expect a smaller quantity of lattice O^{2-} to be active for acrolein formation via the redox pathway. Nevertheless, the secondary discrimination effects at 350, 400, and 450°C for the oxidation of both 1,1,2- d_3 and 2,3,3,3- d_4 propylene resolve this uncertainty and offer conclusive proof that only the redox pathway is operative for propylene oxidation over the β -phase.

The unusual kinetic dependencies and the break in the Arrhenius plot must, therefore, be due to a change in the rate-determining step of the redox pathway. This becomes apparent from the examination of the kinetic isotope effects summarized in Table 4. As expected for the redox pathway, there is no isotope effect for the oxidation of 1,1,2- d_3 propylene, since the methyl group is nondeuterated. However, only partial kinetic isotope effects are obtained for the oxidation of 2,3,3,3- d_4 propylene; only 85, 54, and 35% of the theoretical isotope effects were observed at 450, 400, and 350°C, respectively.

The kinetic isotope effects for the β -phase illustrate that the formation of the symmetric allylic species from propylene in the high-temperature portion of the Arrhenius plot in Fig. 3 is not the only activated process contributing to the value of the reaction rate constant (k_{sp}); this is due to the non-negligible contribution of the process giving rise to the activation energy observed in the low-temperature portion of the Arrhenius curve. Likewise, the presence of 35% of the kinetic isotope effect at 350°C indicates that although some process other than allyl formation is the rate-determining step, the rate constant for allyl formation is non-negligible at 350°C and contributed significantly to the overall reaction rate constant.

The results summarized in Table 6 illustrate the role of allyl formation from propylene for the steady-state oxidation of propylene at 350°C and is accomplished by separating the processes of catalyst reduction and reoxidation. The results of Table 6 show that the initial rate of acrolein formation during the reduction of the β -phase by propylene is essentially the same as the steady-state rate of acrolein formation during the oxidation of propylene. In addition, in the absence of oxygen a full kinetic isotope effect is observed for the initial stages of reduction of β - $Bi_2Mo_2O_9$ by 2,3,3,3- d_4 propylene. Besides offering further proof for the exclusivity of the redox mechanism at 350°C, the full kinetic isotope effect reveals that the low-temperature region of the Arrhenius plot in Fig. 3 includes process(es) related to catalyst reoxidation and not the desorption of adsorbed acrolein, as suggested by Batist *et al.* (23, 24); a rate-limiting step of acrolein desorption would certainly diminish the full kinetic isotope effect of Table 6.

Insight into the nature of the process(es) giving rise to the activation energy of 40.8 kcal/mole for the low-temperature region is gained from the results presented in Table 3. The existence of a small, but significant

kinetic isotope effect for O–O bond breaking reveals that one of the activated processes of reoxidation is dissociation of adsorbed molecular oxygen. The uncertainty of the nature of the molecular oxygen species at the transition state makes it extremely difficult to calculate a theoretical isotope effect, although one would expect a species with negative charge on the oxygen molecule due to the electronegativity of oxygen and the excess electrons present in the reduced catalyst.

The above interpretation is in agreement with Peacock (35, 36) who noted that at temperatures between 325 and 390°C, the ESR signal of Mo^{5+} decreased with increasing temperature (due to formation of Mo^{6+}) during the oxidation of propylene over a bismuth molybdate catalyst, illustrating that catalyst reoxidation was the rate-limiting step at lower temperatures.

For the temperature range between 300 and 350°C in Table 1, the reaction order of oxygen for acrolein formation is approximately 0.5, which also suggests dissociation of adsorbed oxygen in the rate-determining step. This partial order is the same as the value of 0.5 reported by Sancier (37) for the oxidation of an unspecified bismuth molybdate catalyst. More recently, Krenzke and Keulks (6) calculated reaction orders for oxygen of 0.4 for acrolein formation at temperatures between 325 and 375°C over the γ -phase. For the α -phase, however, zero-order kinetics for oxygen pressure were observed and would appear to be due to the failure to examine lower oxygen partial pressures.

Based on the above kinetic and isotopic data, it is apparent that the oxidation of propylene to acrolein over the β -phase proceeds via the redox mechanism. As shown in the earlier paper (5), the following equations can be written:

$$\frac{-d(\text{C}_3\text{H}_6)}{dt} = k_r P_{\text{C}_3}^{-x} \theta_{\text{ox}} \quad (2)$$

$$\frac{-d(\text{O}_2)}{dt} = k_{\text{ox}} P_{\text{O}_2}^y (1 - \theta_{\text{ox}}). \quad (3)$$

Equation (2) denotes the rate of catalyst reduction (which is also equal to the rate of acrolein formation for the redox pathway), and Eq. (3) is the rate of catalyst reoxidation. In addition, k_r and k_{ox} are the rate constants for catalyst reduction and reoxidation, respectively; P_{C_3} and P_{O_2} are the partial pressures of propylene and oxygen, respectively, while x and y are their respective reaction orders. The fraction of sites which is fully oxidized is given by θ_{ox} , while $(1 - \theta_{\text{ox}})$ represents the fraction of vacant, or reduced, sites.

At steady-state reaction conditions, the two processes must occur at the same rate. After equating the two above equations and rearranging, one obtains

$$\theta_{\text{ox}} = \frac{K_{\text{ox}} P_{\text{O}_2}^y}{k_r P_{\text{C}_3}^{-x} + k_{\text{ox}} P_{\text{O}_2}^y} \quad (4)$$

Substitution of (4) into (2) gives

$$\begin{aligned} \frac{-d(\text{C}_3\text{H}_6)}{dt} &= \frac{d(\text{C}_3\text{H}_4\text{O})}{dt} \\ &= k_r P_{\text{C}_3}^{-x} \frac{k_{\text{ox}} P_{\text{O}_2}^y}{k_r P_{\text{C}_3}^{-x} + k_{\text{ox}} P_{\text{O}_2}^y} \quad (5) \end{aligned}$$

which describes the rate of formation of acrolein throughout the complete ranges of temperature and partial pressures of propylene and oxygen.

As a result of the temperature dependence of k_r and k_{ox} , at the highest temperatures $k_{\text{ox}} P_{\text{O}_2}^y > k_r P_{\text{C}_3}^{-x}$ and (5) simplifies to $d(\text{C}_3\text{H}_4\text{O})/dt = k_r P_{\text{C}_3}^{-x}$, where $x = 1.0$ and one obtains the kinetic expression generally associated with propylene oxidation over bismuth molybdate catalysts. Likewise, at the lowest temperatures $k_r P_{\text{C}_3}^{-x} > k_{\text{ox}} P_{\text{O}_2}^y$ and (5) becomes $d(\text{C}_3\text{H}_4\text{O})/dt = k_{\text{ox}} P_{\text{O}_2}^y$, which is observed for the β -phase at 300 and 325°C at an approximate value of $y = 0.5$.

However, at intermediate temperatures the contributions of the partial pressures of propylene and oxygen become significant and it is essential to consider these terms as well as the temperature-dependent k_r and k_{ox} terms when evaluating the kinetic pa-

rameters. In this transition region the observed kinetics are a composite of both reduction and reoxidation kinetics. As a result, intermediate activation energies and partial reaction orders of propylene and oxygen occur. This can be easily seen if Eq. (5) is applied to Fig. 5. During the evaluation of the kinetic dependency of propylene for acrolein formation, the reaction order is zero order in propylene for pressures of 0.1 atm or greater because the relationship $k_r P_{C_3}^{-x} > k_{ox} P_{O_2}^y$ simplifies (5) to $d(C_3H_4O)/dt = k_{ox} P_{O_2}^y$. However, as the propylene pressure is decreased below 0.1 atm, the above relationship no longer holds; rather the propylene dependency approaches first order because $k_r P_{C_3}^{-x} < k_{ox} P_{O_2}^y$.

Likewise, the oxygen dependency for acrolein formation changes from zero to 0.4 order as the oxygen partial pressure decreases from 0.3 atm to 0.03 atm as the relationship $k_{ox} P_{O_2}^y > k_r P_{C_3}^{-x}$ shifts to $k_{ox} P_{O_2}^y < k_r P_{C_3}^{-x}$. A comparison of Figs. 1 and 5 reveals that changing the propylene pressure from a constant value of 0.05 atm to 0.1 atm causes the transition from zero to 0.4 order in oxygen pressure to occur at pressures greater than 0.3 atm oxygen and, thus, explains why Krenzke and Keulks (6) did not observe the changes in reaction order for the α - and γ -phases.

C. Kinetics and Mechanism of Carbon Dioxide Formation

Since it has been stated that CO_2 is formed from the further oxidation of adsorbed acrolein (6, 19–22), one would expect similar kinetic parameters for both acrolein and CO_2 . This was generally found to be the case in this study:

(1) Both acrolein and CO_2 exhibit the same kinetic isotope effects (Table 4) for the oxidation of 2,3,3,3- d_4 propylene and, thus, a common rate-determining step.

(2) The oxygen-18 studies summarized in Table 2 show virtually the same extent of lattice O^{2-} participation for acrolein and

CO_2 formation which indicates that CO_2 is formed via the redox pathway.

(3) Both acrolein and CO_2 have similar kinetic isotope effects at 350°C for molecular oxygen dissociation (Table 3) which illustrate the reoxidation limitations for the formation of both products at low temperatures.

Based on the above, one would expect similar reaction orders for acrolein and CO_2 ; examination of Table 1 shows this is not the case. At temperatures above 425°C, there is a partial order dependency in oxygen for CO_2 formation, but not acrolein. Also, the propylene dependencies for CO_2 formation are not noticeably greater than those for acrolein formation at all temperatures and are, in fact, higher than 1.0 at temperatures of 425°C and above. Reaction orders greater than 1.0 for olefins in heterogeneously catalyzed reactions are unusual. Baryshevaskaya *et al.* (38, 39), however, reported reaction orders of 1.5 for propylene and 0.5 for oxygen using a Co–Bi–Mo oxide catalyst between 425 and 480°C and stated the observed kinetics were due to the presence of both consecutive and parallel pathways of propylene oxidation to CO_2 . This explanation is incomplete if both the consecutive and parallel pathways are first order in propylene pressure, since the sum of both of these pathways is simply a cumulative pathway of first-order propylene kinetics. Observation of a reaction order greater than 1.0 implies the presence of more than one molecule of propylene in the transition state of the rate-determining step.

Krenzke and Keulks (6) also noted partial oxygen reaction orders for CO_2 formation at temperatures in which the oxygen dependency for acrolein formation was zero for the α - and γ -phases, although the reaction orders of propylene for both products did not exceed 1.0.

A reasonable explanation for the CO_2 kinetics can be developed from the results in Table 7, which reveal the presence of a significant hydrocarbon build-up on the

steady-state surface of the β -phase over the temperature range investigated in this study. Oxidation of this hydrocarbon deposit by oxygen formed only CO_2 and H_2O , an indication that the surface deposit was a hydrocarbon and not solely carbonaceous. The oxygen dependencies for CO_2 formation, which were found to be 0.3 and 0.25 at 350 and 425°C, respectively, explain the partial oxygen dependency for CO_2 formation at high temperatures. The propylene dependencies were not determined since there was no direct way to determine the rate of hydrocarbon build-up. However, the observed propylene dependencies of 1.0–1.5 and the kinetic isotope effects can be readily explained if the hydrocarbon deposit is formed by the interaction of two allyl-like species (or two different hydrocarbon or oxidation products) in the transition state of the rate-determining step of this build-up process.

This interpretation is consistent with the work of Kobayaski and Futaya (40) who found that the pathway to CO_2 involves the formation of a stable surface intermediate. The surface intermediate is formed from propylene after the formation of the allylic species and also from acrolein. No CO_2 is formed directly from propylene.

This interpretation also is in excellent agreement with the results reported by Grzybowska *et al.* (41), who used XPS to examine the surfaces of the α -, β -, and γ -phases after the steady-state oxidation of propylene at 440°C and found a sizable oxygenated hydrocarbon build-up on the surfaces of all three phases. Degassing at 430°C for 12 hr did not remove the strongly bound surface deposit.

Replacement of the $^{16}\text{O}_2$ by $^{18}\text{O}_2$ in the feed stream (Table 7) demonstrates that the oxygen incorporated into the CO_2 comes from the lattice and not the gas phase. Thus, the oxygen in the feed stream indirectly oxidizes the surface build-up. This is somewhat surprising, yet consistent with earlier oxygen-18 results (Table 2) which

reveal that CO_2 is produced exclusively by the redox pathway. Also, the existence of similar kinetic isotope effects for acrolein and CO_2 from the oxidation of 2,3,3,3- d_4 propylene shows the hydrocarbon deposit is produced after the formation of the allylic species.

Based on the above data, the overall rate of CO_2 formation can be stated as

$$d(\text{CO}_2)/dt = k_{\text{CO}_2} \theta_{\text{C}_3\text{H}_4\text{O}} \theta_{\text{ox}} + k'_{\text{CO}_2} P_{\text{O}_2}^{0.3} \Phi_{\text{ss}} \quad (6)$$

where k_{CO_2} and k'_{CO_2} are the formation rate constants, $\theta_{\text{C}_3\text{H}_4\text{O}}$ is the surface coverage of adsorbed acrolein and is directly proportional to $P_{\text{C}_3\text{H}_6}^x$, θ_{ox} is the fraction of oxidized surface sites, Φ_{ss} is the steady-state coverage of strongly bound hydrocarbon, and $P_{\text{O}_2}^{0.3}$ is the kinetic dependency for oxidation of the surface.

At lower temperatures (below 400°C) the first term (on the right-hand side) in Eq. (6) is primarily responsible for CO_2 formation by the further oxidation of adsorbed acrolein. At temperatures greater than 400°C, the second term in Eq. (6) contributes significantly to CO_2 formation, which results in a complex rate equation and a kinetic dependency of propylene greater than 1.0.

In summary, the selective oxidation of propylene to acrolein over the β -phase occurs exclusively by the redox mechanism, and the kinetics and energetics of acrolein formation can be completely described in terms of the coupled kinetics of catalyst reduction and reoxidation. The formation of CO_2 is a more complex process than the oxidation of adsorbed acrolein. At higher temperatures, where the desorption of acrolein is not as critical, a significant fraction of CO_2 is produced by the oxidation of a strongly bound hydrocarbon deposit.

REFERENCES

1. Voge, H. H., and Adams, C. R., *Adv. Catal.* **17**, 151 (1967).
2. Sachtler, W. M., *Catal. Rev.* **4**, 26 (1970).
3. Margolis, L. Ya., *Catal. Rev.* **8**, 241 (1973).

4. Keulks, G. W., Krenzke, L. D., and Notermann, T. M., *Adv. Catal.* **27**, 183 (1978).
5. Krenzke, L. D., and Keulks, G. W., *J. Catal.* **61**, 316 (1980).
6. Krenzke, L. D., and Keulks, G. W., *J. Catal.* **64**, 295 (1980).
7. Batist, Ph. A., DerKinderen, A. H. W. M., Leeuwenburgh, Y., Metz, F. A. M. G., and Schuit, G. C. A., *J. Catal.* **12**, 45 (1968).
8. Rashkin, J., and Pierron, E. D., *J. Catal.* **6**, 332 (1966).
9. Kohlmuller, R., and Baduad, J. P., *Bull. Chem. Soc. Chim.* **10**, 3434 (1969).
10. Erman, L. Ya., and Gal'perin, E. L., *Russ. J. Inorg. Chem.* **11**, 122 (1966).
11. Erman, L. Ya., and Gal'perin, E. L., *Russ. J. Inorg. Chem.* **13**, 487 (1968).
12. Erman, L. Ya., and Gal'perin, E. L., *Russ. J. Inorg. Chem.* **15**, 441 (1970).
13. Monnier, J. R., Ph.D. Thesis, University of Wisconsin—Milwaukee, 1978.
14. Kugler, B. L., and Kokes, R. J., *J. Catal.* **32**, 170 (1974).
15. Kugler, B. L., and Gryder, J. W., *J. Catal.* **44**, 126 (1976).
16. Cant, N. W., and Hall, W. K., *J. Catal.* **22**, 310 (1971).
17. Cant, N. W., and Hall, W. K., *J. Phys. Chem.* **75**, 2914 (1971).
18. Daniel, C., Monnier, J. R., and Keulks, G. W., *J. Catal.* **31**, 360 (1973).
19. Keulks, G. W., Rosynek, M. P., and Daniel, C., *Ind. Eng. Chem. Prod. Res. Develop.* **10**, 138 (1971).
20. Gorshkov, A. P., Kolchin, I. K., Gribov, I. M., and Margolis, L. Ya., *Kinet. Katal.* **9**, 1086 (1968).
21. Gorshkov, A. P., Kolchin, I. K., Isgulyants, G. V., Derbentsev, Ya. I., and Margolis, L. Ya., *Dokl. Akad. Nauk SSSR* **186**, 827 (1969).
22. Gargarin, S. G., Kolchin, I. K., and Margolis, L. Ya., *Neftekhimiya* **10**, 59 (1970).
23. Batist, Ph. A., Bouwens, J. F. H., and Schuit, G. C. A., *J. Catal.* **25**, 1 (1972).
24. Keizer, K., Batist, Ph. A., and Schuit, G. C. A., *J. Catal.* **15**, 256 (1969).
25. Sancier, K. M., Wentrcek, P. R., and Wise, H., *J. Catal.* **39**, 141 (1975).
26. Grzybowska, B., Haber, J., and Komorek, J., *J. Catal.* **25**, 25 (1972).
27. Melander, L., "Isotope Effects on Reaction Rates," pp. 7-22. Ronald Press, New York, 1960.
28. Herzberg, G., "Spectra of Diatomic Molecules," p. 98. Van Nostrand, Princeton, 1950.
29. Rolfe, J., Holzer, W., Murphy, W. F., and Bernstein, H. J., *J. Chem. Phys.* **49**, 963 (1968).
30. Creighton, J. A., and Lippincott, E. R., *J. Chem. Phys.* **40**, 1779 (1964).
31. Evans, J. C., *J. Chem. Soc. D.* 682 (1969).
32. Adams, D. M., "Metal Ligand and Related Vibrations," p. 258. St. Martin's Press, New York, 1968.
33. Keulks, G. W., and Daniel, C., *J. Catal.* **24**, 529 (1971).
34. Haber, J., and Grzybowska, B., *J. Catal.* **28**, 489 (1973).
35. Peacock, J. M., Parker, A. J., Ashmore, P. G., and Hockey, J. A., *J. Catal.* **15**, 373 (1969).
36. Peacock, J. M., Parker, A. J., Ashmore, P. G., and Hockey, J. A., *J. Catal.* **15**, 379 (1969).
37. Sancier, K. M., Aoshima, A., and Wise, H., *J. Catal.* **34**, 257 (1974).
38. Baryshevskaya, I. M., Kholyavenko, K. M., and Rubanik, M. Ya., *Ukr. Khim. Zh.* **35**, 702 (1969).
39. Baryshevskaya, I. M., Kholyavenko, K. M., and Rubanik, M. Ya., *Ukr. Khim. Zh.* **35**, 805 (1969).
40. Kobayaski, M., and Futaya, R., *J. Catal.* **56**, 73 (1979).
41. Grzybowska, B., Haber, J., Marczewski, W., and Ungier, L., *J. Catal.* **42**, 327 (1976).
42. Egashira, M., Sumie, H., Sakamoto, T., and Seiyama, T., *Chem. Soc. Japan* **73**, 860 (1970).
43. Roiter, V. A., Golodets, G. I., and Pyatnitskii, Yu. I., *Proc. Fourth Int. Congr. Catal. Moscow, 1968* **1**, 466 (1970).
44. Boreskov, G. K., Popvskii, V. V., and Sazonov, V. A., *Proc. Fourth Int. Congr. Catal. Moscow, 1968* **1**, 439 (1971).